



# CHORUS

This is the accepted manuscript made available via CHORUS. The article has been published as:

## Magnetic properties and magnetic structures of $\text{TbBaMn}_2\text{O}_{5.75}$ : Possible observation of unconventional polaron trimers

Graham King, Anna Llobet, and Susana Garcia-Martin

Phys. Rev. B **91**, 024412 — Published 12 January 2015

DOI: [10.1103/PhysRevB.91.024412](https://doi.org/10.1103/PhysRevB.91.024412)

# The Magnetic Properties and Magnetic Structures of $\text{TbBaMn}_2\text{O}_{5.75}$ : Possible Observation of Unconventional Polaron Trimers

Graham King,<sup>1</sup> Anna Llobet,<sup>1</sup> Susana Garcia-Martin<sup>2</sup>

<sup>1</sup> *Lujan Neutron Scattering Center, Los Alamos National Laboratory, MS H805, Los Alamos, NM 87545, USA*

<sup>2</sup> *Departamento de Química Inorgánica, Facultad de C.C. Químicas, Universidad Complutense, 28040-Madrid, Spain*

## Abstract

The magnetism of the oxygen deficient, *A*-site layered perovskite  $\text{TbBaMn}_2\text{O}_{5.75}$  has been studied by magnetic susceptibility vs. temperature measurements and neutron powder diffraction. Four magnetic phases have been identified. Above 457 K a charge melted state exists where ferromagnetic double exchange interactions between the Mn ions dominate. Below 457 K charge ordering occurs and the exchange interactions become primarily antiferromagnetic. The magnetic moment in this phase is too large to be consistent with a charge ordering of  $\text{Mn}^{3+}$  and  $\text{Mn}^{4+}$  but could be explained by having 2  $e_g$  electrons being shared among 3 Mn centers, causing them to act as a single paramagnetic unit. This suggests that  $S = 11/2$   $(\text{Mn}^{3.33+})_3$  polaron trimers may be present along with  $\text{Mn}^{3+}$ . Below 203 K long range ordering of the moments on the Mn ions occurs. Neutron powder diffraction data at 52 K reveal a magnetic structure containing an  $\uparrow\uparrow\downarrow$  pattern of spins which is consistent with the formation of tripolarons. Below 11 K the  $\text{Tb}^{3+}$  ions also undergo long range magnetic ordering.

## 1. Introduction

The search for new multiferroic materials, those which exhibit both ferroelectricity and magnetic order, has been largely driven by their many potential uses in electronic devices. Multiferroic materials are uncommon since the type of cations which tend to undergo the off-center displacements which produce ferroelectricity (highly charge  $d^0$  transition metals such as  $Ti^{4+}$  and  $Nb^{5+}$  or heavy lone pair cations such as  $Pb^{2+}$  and  $Bi^{3+}$ ) lack the unpaired electrons necessary for magnetism.<sup>1-5</sup> Multiferroic materials which have a strong coupling between the electronic and magnetic order parameters are even less common. Many of the known multiferroics use two different cations, one which produces the ferroelectricity and the other which produces the magnetism, but in these cases there is no mechanism to couple these orders. However, strong magnetoelectric coupling is highly desired for most of the applications such as electric field-controlled magnetic devices. This has led to a search for materials which achieve multiferroic behavior by novel mechanisms which will strongly couple the order parameters. These include achieving ferroelectricity through spiral magnetic ordering or charge ordering.<sup>6-9</sup> Efremov and co-workers have predicted that coupling between magnetic and charge ordering in charge-ordered (CO) and orbital-ordered perovskites can give rise to ferroelectric magnetism.<sup>10</sup> They propose different types of charge ordering in doped manganites: site-centered CO and bond-centered CO. A bond-centered CO model, named “Zener polaron”, was suggested in  $Pr_{0.6}Ca_{0.4}MnO_3$  for the first time from crystallographic results.<sup>11</sup> The symmetry of the crystal structure of this compound, which is non-centrosymmetric ( $P11m$ ), and its magnetic properties seemed to indicate multiferroic behavior. Subsequent studies have experimentally evidenced that charge-ordered rare earth manganites such as  $Nd_{0.5}Ca_{0.5}MnO_3$ ,  $Pr_{0.7}Ca_{0.3}MnO_3$  and  $Gd_{0.5}Sr_{0.5}MnO_3$ <sup>12, 13</sup> possess multiferroic and magnetoelectric properties. These results clearly point out that charge-ordering provides a novel route to multiferroic properties especially in the case of the manganites.

High CO-transition temperatures ( $T_{CO}$ ) are found in  $A$ -site ordered perovskites of the system  $RBaMn_2O_6$  ( $R = Y$  and lanthanide elements).<sup>14-16</sup> The very high  $T_{CO}$  (close to 500 K) is related to the layered-type ordering of  $R$  and Ba cations. Moreover, the  $A$ -site ordering induces new combinations between the spin, charge and orbital degrees of freedom. CO-structures have been experimentally evidenced by several techniques and different CO models have been proposed in some of these  $RBaMn_2O_6$  perovskites.<sup>17-22</sup>

$TbBaMn_2O_{5.75}$  has a complex structure which indicates the potential for multiferroic behavior.<sup>23</sup> This compound has a perovskite type structure where the Tb and Ba ions are ordered into alternated  $(001)_p$  layers perpendicular to the  $c$  lattice parameter. In addition to the Tb and Ba cation ordering, charge ordering and oxygen vacancy ordering have been proposed in  $TbBaMn_2O_{5.75}$  creating a  $\sqrt{2}a_p \times 2\sqrt{2}a_p \times 4a_p$  unit cell ( $a_p$  refers to the lattice parameter of the cubic perovskite structure). Exit wave reconstruction of high resolution transmission electron microscopy (HRTEM) images reveals that the oxygen vacancies are located exclusively within the Tb layer. Charge ordering, that exists well above room temperature, has been proposed to

consist of three stripes of  $\text{Mn}^{3+}$  alternating with one stripe of  $\text{Mn}^{4+}$  along the  $[110]_p$  direction within the  $(001)_p$  planes. CO bilayers of this type, shifted by  $2a_p$  along the  $[100]_p$  direction every other layer, are located along  $[001]_p$ . What is of particular relevance is that the combination of both the layered cation ordering and charge ordering breaks the inversion symmetry leading to a polar space group ( $P22_12_1$ ). Since the charge ordering of magnetic cations directly leads to the loss of inversion symmetry, the ferroelectricity and magnetism can be expected to be naturally coupled.

In this study the magnetism of  $\text{TbBaMn}_2\text{O}_{5.75}$  has been examined in detail by magnetic susceptibility vs. temperature measurements and neutron powder diffraction measurements collected over broad temperature ranges. These measurements both indicate that the nature of the charge ordering is different than originally proposed. The evidence indicates that the charge ordering likely consists of ferromagnetically coupled  $(\text{Mn}^{3.33+})_3$  trimer polarons and  $\text{Mn}^{3+}$  in a 1:1 ratio.

## 2. Experimental

The synthesis of this compound has been reported previously.<sup>23</sup> Zero field cooled magnetic susceptibility data were collected on a SQUID magnetometer MPMS-XL (Quantum Design Co.) using an applied magnetic field of 0.1 T. Two data sets were collected using different experimental setups, one ranging from 2-299 K and the other from 300-699K.

Time-of-flight neutron powder diffraction data were collected on the HIPD instrument at the Lujan Neutron Scattering Center of Los Alamos National Laboratory. Fifteen data sets were collected at temperatures ranging from 4-300 K. Rietveld refinements were done using the GSAS/EXPGUI software package.<sup>24,25</sup> The refinements of the magnetic structures were done using the program *SARAH* along with GSAS.<sup>26</sup>

## 3. Results and Discussion

**3.1 Magnetic Phases.** The magnetic susceptibility vs. temperature data (Fig. 1) indicate that  $\text{TbBaMn}_2\text{O}_{5.75}$  passes through three magnetic phase transitions in the temperature range of 2-699 K. Above 457 K a charge melted (CM) paramagnetic (PM) state exists and below this temperature there is a phase transition to a charge ordered (CO) PM state. At 203 K long range ordering of the Mn moments occurs, followed by long range ordering of the Tb moments at 11 K.

The sharp peak observed in the magnetic susceptibility data at 457 K can be ascribed to the transition from the CM PM state to the CO PM state. A Curie-Weiss (CW) fit was done on the  $1/\chi$  data over the range of 501-699 K (Fig. S1 in the supporting information<sup>27</sup>) to extract the

magnetic moment and Weiss constant ( $\theta$ ) for the CM phase. The linear fit is essentially perfect, indicating ideal PM behavior in this temperature range. Values extracted from the CW fits are given in Table 1. All magnetic moments are reported per a  $\text{Tb}_2\text{Ba}_2\text{Mn}_4\text{O}_{11.5}$  formula unit since this is the smallest unit that accounts for the  $3e_g$  electrons per 4 Mn ions ratio. The CW fit gives a magnetic moment of  $15.04(2) \mu\text{B}$  and a large positive  $\theta$  of  $196.4(8) \text{ K}$ . The Weiss constant has contributions from Mn-Mn, Mn-Tb, and Tb-Tb magnetic exchange interactions. It can be expected that the Mn-Mn interactions are much stronger than the other two types of coupling and determine the sign of  $\theta$ . The positive  $\theta$  therefore indicates that the Mn ions are ferromagnetically (FM) coupled in the CM phase. The FM interactions between the Mn can be explained in terms of double exchange. The average oxidation state of Mn in this sample has been previously determined to be  $3.24(6)$ .<sup>23</sup> Each Mn ion has 3 electrons localized in  $t_{2g}$  orbitals. In addition, there are also 3 electrons per 4 Mn ions which are delocalized throughout the  $e_g$  orbitals of all Mn ions. In order for these electrons to delocalize the  $t_{2g}$  electrons on the Mn ions should all be of the same spin direction in order to obey Hund's rules, leading to FM interactions. The observed moment of  $15.04(8)$  is smaller than expected, considering the theoretical moment for 2  $\text{Tb}^{3+}$ , 3  $\text{Mn}^{3+}$ , and 1  $\text{Mn}^{4+}$  is  $16.61 \mu\text{B}$ . The reduced moment can be explained by the itinerant nature of the  $e_g$  electrons. Since the  $e_g$  electrons are not localized they do not contribute to CW paramagnetism but instead make a much smaller Pauli paramagnetic contribution. If the  $e_g$  electrons are completely neglected a moment of  $15.78 \mu\text{B}$  would be expected. This value is only slightly larger than the experimental one and the difference can be explained in terms of diamagnetism and experimental errors.

Below the CO temperature the nature of the magnetic interactions fundamentally changes. The  $1/\chi$  data below 457 K is highly non-linear until  $\sim 350 \text{ K}$ , indicating that the magnetic interactions are continuously changing over this temperature range. The  $1/\chi$  data from 224-299 K can be fit to the CW law and is perfectly linear, indicating that over this temperature range ideal PM behavior is observed (Fig. S2). One of the most striking differences between the CM and the CO phase is that the sign of the Weiss constant has changed. The negative  $\theta$  of  $-75.6(5) \text{ K}$  indicates that the Mn-Mn exchange interactions are primarily antiferromagnetic (AFM) in the CO phase. The moment has also increased substantially to  $18.49(3) \mu\text{B}$ . While we previously proposed a charge ordering of 3  $\text{Mn}^{3+}$  and 1  $\text{Mn}^{4+}$  for the CO phase,<sup>23</sup> the observed moment for this phase is about 11.3% larger than the  $16.61 \mu\text{B}$  expected for such a situation. Increased moments have been observed previously in manganates and have been attributed to the formation of Zener polarons.<sup>11,28</sup> Zener bipolarons occur when a  $\text{Mn}^{3+}$  and  $\text{Mn}^{4+}$  couple by sharing the one  $e_g$  electron between them. This FM couples them and causes them to act as a single  $S = 7/2$  species, which contributes a larger moment than two separate  $S = 2$  and  $S = 3/2$  species. If it is assumed that there are 2  $\text{Tb}^{3+}$ , 2  $\text{Mn}^{3+}$  and 1  $S=7/2$  bipolaron pair then a theoretical moment of  $17.32 \mu\text{B}$  is obtained. While this is an improvement it is still somewhat less than the observed moment. If instead it is assumed that 3 Mn ions share 2  $e_g$  electrons to form  $(\text{Mn}^{3.33+})_3$  trimers then an even larger moment would be obtained. The theoretical moment for 2  $\text{Tb}^{3+}$ , 1  $\text{Mn}^{3+}$  and 1  $S= 11/2$  trimer is  $18.87 \mu\text{B}$ . This is only 2% larger than the observed

moment of 18.49(3)  $\mu\text{B}$  and can be regarded as an almost perfect match since the diamagnetic correction has not been taken into account for this calculation. The formation of FM coupled trimers is also consistent with the magnetic structure, as discussed later on. If  $S = 15/2$  tetramers were formed by 4 Mn sharing 3  $e_g$  electrons then a theoretical moment of 21.07  $\mu\text{B}$  would be obtained, which is much larger than the actual moment. These results suggest that the CM to CO phase transition does not involve the formation of 3  $\text{Mn}^{3+}$  per 1  $\text{Mn}^{4+}$  but instead involves the formation of  $(\text{Mn}^{3.33+})_3$  polarons, leaving some  $\text{Mn}^{3+}$ . The CM to CO transition could be described as a switch from the  $e_g$  electrons on the Mn being completely delocalized to pairs of them becoming localized on trimers of Mn ions and single  $e_g$  electrons localizing on  $\text{Mn}^{3+}$ .

As the temperature is further lowered the  $1/\chi$  curve does not stay linear but begins to change slope. By taking the first derivative of this function a phase transition temperature of 203 K can be assigned (Fig. S3). This phase transition can be attributed to long range AFM ordering of the  $\text{Mn}^{3+}$  and the  $(\text{Mn}^{3.33+})_3$  trimers, while the  $\text{Tb}^{3+}$  remains PM. While the  $1/\chi$  curve is not linear around this transition temperature, it becomes nearly linear at lower temperature. A CW fit was done on the  $1/\chi$  data ranging 61-126 K (Fig. S4). The data in this region is far from phase transitions and is very close to linear. The magnetic moment has now been reduced to 15.4(1)  $\mu\text{B}$  as a result of the long range AFM ordering of the Mn moments. This value is above the expected value of 13.75  $\mu\text{B}$  for 2  $\text{Tb}^{3+}$  ions. It can be expected that the AFM aligned Mn ions still contribute a small amount to the susceptibility, increasing the moment and causing the slight deviation from linearity in  $1/\chi$ . The  $\theta$  value is also now only -11.4(5) K. While the CW law is not strictly valid in this temperature range due to the presence of the AFM ordered Mn ions, this  $\theta$  value can be considered the approximate Weiss temperature of the Tb sub-lattice resulting from both Mn-Tb and Tb-Tb interactions.

A second AFM transition is observed at 11 K where the susceptibility peaks and then begins to decrease as the temperature is further lowered. This transition temperature represents the longer range magnetic ordering temperature of the  $\text{Tb}^{3+}$  ions and is in excellent agreement with the  $\theta$  value obtained for the phase where only the  $\text{Tb}^{3+}$  are paramagnetic.

**3.2 Variable Temperature NPD Studies.** As discussed in previous work, while the combinations of Tb/Ba ordering, oxygen vacancy ordering, and charge ordering in  $\text{TbBaMn}_2\text{O}_{5.75}$  leads to a large orthorhombic supercell with dimensions of  $\sim 5.5\text{\AA} \times \sim 11.0\text{\AA} \times \sim 15.2\text{\AA}$  ( $\sqrt{2}a_p \times 2\sqrt{2}a_p \times 4a_p$ ), the subcell metrics are highly pseudo-tetragonal and all of the major peaks in the neutron powder diffraction (NPD) patterns can be fit using a simple  $\sim 3.9\text{\AA} \times \sim 3.9\text{\AA} \times \sim 7.6\text{\AA}$  ( $a_p \times a_p \times 2a_p$ ) tetragonal subcell.<sup>23</sup> There are only a few very weak peaks in the NPD patterns that arise from the true larger supercell. The NPD patterns taken at all temperatures have been fit with the tetragonal subcell in order to extract the lattice parameters, which are given in Table 2. It is observed that as the sample is cooled the  $c$  lattice parameter (perpendicular to the Tb/Ba layered ordering) contracts much more rapidly than does the  $a$  lattice parameter.

The NPD patterns collected at 300, 240, and 200 K show only nuclear peaks. Upon cooling to 175 K new peaks appear which can be ascribed to the onset of long range magnetic ordering. This is in good agreement with the susceptibility data which indicate that the Mn moments begin to order around 203 K. The intensities of the magnetic peaks grow slowly and steadily in the NPD patterns as the temperature is lowered down to 15 K but increase much more rapidly in the NPD patterns taken at 10 and 4 K due to the ordering of the  $Tb^{3+}$ .

**3.3 Magnetic Structure at 52 K.** The NPD pattern collected at 52 K was used to determine the magnetic structure at a temperature where only the Mn moments are ordered. The nuclear phase was fit using the tetragonal sub-structure which was able to fit all but a few very weak peaks. The actual positions of the Mn atoms should be very close to these idealized positions as the intensities of the nuclear peaks are well fit. The weak supercell peaks are at low enough d-spacing that magnetic scattering should be negligible and so they should not interfere with the determination of the magnetic structure. The indexing of the magnetic structure was based on the actual orthorhombic supercell.

The magnetic reflections could not all be indexed using just a single propagation vector. Almost every magnetic peak could be indexed using a propagation vector of  $k = (\frac{1}{2}, 0, 0)$ , producing a magnetic unit cell of dimensions  $11.035 \text{ \AA} \times 11.035 \text{ \AA} \times 15.122 \text{ \AA}$  ( $2\sqrt{2}a_p \times 2\sqrt{2}a_p \times 4a_p$ ). The only peak not indexed by this propagation vector is a very weak peak at  $\sim 15.1 \text{ \AA}$  which is barely detectable above the background noise. This peak requires a  $k = (0, 0, 0)$  propagation vector in order for it to have intensity. The  $k = (0, 0, 0)$  component of the magnetic structure is too small to be meaningfully refined, but it should be kept in mind that the true magnetic structure has small perturbations from the idealized  $k = (\frac{1}{2}, 0, 0)$  structure presented below.

The magnetic structure determination was done using representational analysis with the program *SARAh*. There are 32 Mn atoms in the magnetic unit cell corresponding to 4 symmetrically unique Mn atoms all with multiplicities of 8. The representational analysis produced four irreducible representations (IRs) each with three basis vectors. Not all peaks allowed by the  $k = (\frac{1}{2}, 0, 0)$  vector are observed in the NPD pattern. The basis vectors were each examined to see which ones produced magnetic intensity only at the observed peak positions. Of the 12 basis vectors only 3 ( $\psi_3, \psi_5, \psi_7$ ) fulfilled this condition. A large number of simulated annealing runs were done in *SARAh* using these basis vectors to explore the possible magnetic structures. If the moments were constrained to be collinear then only a single unique structure was obtained. If the moments of all the atoms were allowed to refine freely highly complex non-collinear solutions could be obtained, however these seem much less likely than the collinear solution and were discarded. The final fit to the NPD data is shown in Figure 2.

The magnetic structure is shown in Figure 3. Within the  $ab$ -plane there are  $\uparrow\uparrow\uparrow\downarrow$  and  $\downarrow\downarrow\downarrow\uparrow$  patterns of the moments along both the  $[110]$  and  $[-110]$  directions (the  $[100]$  and  $[010]$  directions of the ideal cubic perovskite). These layers are shifted by  $(\frac{1}{2}, \frac{1}{2})$  each layer along the

$z$ -axis, producing an  $\uparrow\uparrow\downarrow\downarrow$  pattern in this direction. The  $\uparrow\uparrow\downarrow\downarrow$  chains running along the  $z$ -axis are staggered relative to their neighboring chains. The refinements were not particularly sensitive to the directions of the moments, giving similar fits for very different moment directions. The best fits consistently had nearly equal  $x$  and  $y$  components but only small  $z$  components. This suggests that the moments lie within or close to within the  $ab$ -plane, although this result must be taken with caution since the moment directions are not well determined. During the early stages of the refinements all Mn ions were constrained to have equal moments, but during the final stages one of the crystallographically unique Mn atoms was allowed to have a different moment than the other three since this is what was expected from the charge ordering. The moment for the majority of the Mn (corresponding to the  $\text{Mn}^{3.33+}$ ) refined to 2.31(3)  $\mu\text{B}$  and the moment for the minority of Mn (corresponding to  $\text{Mn}^{3+}$ ) refined to 2.65(4)  $\mu\text{B}$ . These moments are significantly less than the saturation moments of 3.67  $\mu\text{B}$  and 4  $\mu\text{B}$ , respectively.

The pattern of spins determined from the refinements of the NPD data are difficult to rationalize in terms of superexchange between charge and orbitally ordered  $\text{Mn}^{3+}$  and  $\text{Mn}^{4+}$ , but can be explained by the formation of tripolarons as indicated by the magnetic susceptibility data. The magnetic structure can be thought of as consisting of stripes of  $(\text{Mn}^{3.33+})_3$  trimers going along the [100] or [010] directions, separated by stripes of  $\text{Mn}^{3+}$  (Fig 4). The trimers are always AFM aligned with other neighboring trimers within the  $ab$ -plane. Along the  $c$ -axis the trimers are sometimes AFM and sometimes FM with each other. The  $\text{Mn}^{3+}$  are isolated from each other and have only Mn atoms belonging to trimers as nearest neighbors. The  $\text{Mn}^{3+}$  are AFM aligned with three of these neighbors and FM aligned with the other three. Which directions produce AFM and FM alignment for the  $\text{Mn}^{3+}$  probably depends on the orientation of the occupied  $e_g$  orbital, which is likely ordered in this structure. If the trimers are considered as single magnetic units, then overall there are more AFM relationships in this structure than FM relationships, which is consistent with the negative  $\theta$  obtained from the susceptibility data. Since there is an  $\uparrow\uparrow\downarrow\downarrow$  or  $\downarrow\downarrow\uparrow\uparrow$  pattern of the moments along both the [110] and [-110] directions there are two possible ways to assign the trimers. From the data available it is not possible to choose in which direction they point. Precise Mn–Mn distances would be helpful in making this assignment, but due to the very high pseudo-symmetry and large number of atomic parameters the exact crystal structure has not been able to be solved from the powder diffraction data available. Single crystal experiments would be helpful in this regard. If the  $P22_12_1$  space group symmetry assignment is correct, then the direction which the trimers point should switch every other layer along  $c$ . Otherwise, symmetrically equivalent Mn atoms would be required to be both  $\text{Mn}^{3.33+}$  and  $\text{Mn}^{3+}$ . If the direction of trimer formation switches every other layer then just one of the symmetrically unique Mn can always be the  $\text{Mn}^{3+}$ . The proposed pattern of tripolaron formation is shown in Figure 4.

**3.4 Magnetic Structure at 4 K.** Upon cooling from 52 K to 4 K the intensities of some of the magnetic reflections, such as the [110] and [111], increase sustainably while others, such as the [130] and [211], remain essentially the same (Fig. 5). No new peaks are produced as a result of

the ordering of the Tb moments. The primary propagation vector still appears to be  $k = (\frac{1}{2}, 0, 0)$ . The intensity of the peak at  $\sim 15.1 \text{ \AA}$ , while still quite small, has increased substantially and is now clearly resolved above the background. This would seem to indicate that there is a significant  $k = (0, 0, 0)$  component to the magnetic structure at 4 K.

Despite extensive efforts to determine the arrangement of the Tb moments using the  $k = (\frac{1}{2}, 0, 0)$  vector as well as several other possible propagation vectors, no satisfactory fits could be obtained. This would seem to indicate the pattern of the  $\text{Tb}^{3+}$  moments is rather complex. In other related perovskites which have layers of  $\text{Tb}^{3+}$  alternating with layers of non-magnetic *A*-site cations it has been shown that Mn-Tb interactions are the dominate force driving the ordering of the  $\text{Tb}^{3+}$ . For example, in  $\text{NaTbMnWO}_6$  the  $\text{Tb}^{3+}$  are found to order at 15 K, but when the  $\text{Mn}^{2+}$  is replaced by the non-magnetic  $\text{Mg}^{2+}$  to form  $\text{NaTbMgWO}_6$  no ordering of the  $\text{Tb}^{3+}$  occurs down to 2 K.<sup>29-31</sup> While the arrangement of the  $\text{Tb}^{3+}$  moments in  $\text{TbBaMn}_2\text{O}_{5.75}$  was not able to be solved, it is clearly different than what is found in  $\text{NaTbMnWO}_6$ . This supports the idea that Mn-Tb interactions are more important than Tb-Tb interactions in determining the magnetic structure of the  $\text{Tb}^{3+}$  sub-lattice.

**3.5 Discussion.** Both the magnetic susceptibility and NPD data are consistent with the formation of tripolarons in  $\text{TbBaMn}_2\text{O}_{5.75}$ . There are several features unique to this particular pattern of polaron formation. While most reported occurrences of polaron formation in manganites are of bipolaron formation in half-doped compositions, it has been suggested that tripolaron formation occurs in compounds such as  $\text{La}_{1/3}\text{Ca}_{2/3}\text{MnO}_3$ .<sup>32</sup> However, in these cases there is only one  $e_g$  electron being shared between the 3 Mn centers, producing  $(\text{Mn}^{3.67+})_3$  trimers with spin  $S = 5$ . To the best of our knowledge, this is the first observation of  $(\text{Mn}^{3.33+})_3$  trimers where the 3 Mn ions share 2  $e_g$  electrons to form  $S = 11/2$  species. Another case of 2  $e_g$  electrons being shared among several Mn atoms has been reported in another *A*-site ordered perovskite,  $\text{YBaMn}_2\text{O}_6$ .<sup>33</sup> In this compound 4 Mn ions share 2  $e_g$  electrons, resulting in the formation of  $S = 7$  tetramers. However, polaron formation does not seem to be a universal feature of *A*-site ordered perovskites as it is reported not to occur in other closely related compositions.<sup>34,35</sup> Tripolaron formation has not been observed in other compounds with average Mn oxidation states of 3.25+, such as  $\text{La}_{3/4}\text{Ca}_{1/4}\text{MnO}_3$ , or in non-manganite perovskites with similar chemical formulas such as  $\text{PrBaCo}_2\text{O}_{5.75}$ .<sup>36,37</sup> Another unusual feature of  $\text{TbBaMn}_2\text{O}_{5.75}$  is the coexistence of multi-center polarons and Mn ions which do not belong to polarons. Usually in manganites all Mn ions participate in the formation of polarons if polarons exist at all, but in this case polaron trimers seem to coexist with isolated  $\text{Mn}^{3+}$ .

The existence of FM coupled trimers of Mn could help to explain some previously confusing structural aspects of  $\text{TbBaMn}_2\text{O}_{5.75}$ . In particular, it has been observed that the superstructure of  $\text{TbBaMn}_2\text{O}_{5.75}$  which results from the charge ordering involves only very subtle displacements of atoms. The superstructure is not detectable by laboratory X-ray diffraction, only barely detectable by NPD, and has only clearly been seen by selected area electron diffraction (SAED) and HRTEM. This is unexpected due to the Jahn-Teller nature of  $\text{Mn}^{3+}$ ,

which should produce Mn–O bonds of much different lengths, leading to a pronounced superstructure. Neutron PDF analysis has confirmed that the Mn–O bond length distribution is narrower than would be expected when 75% of the Mn are in the +3 oxidation state.<sup>23</sup> This was explained by suggesting that the oxygen vacancies preferentially occur around Mn<sup>3+</sup> making them only 5 coordinate, which eliminates one of the long Mn–O bonds and shortens the length of the other. However, with such a low oxygen vacancy concentration this would still leave many long Mn–O bonds since 75% of the Mn are in the +3 oxidation state. It has been observed for half doped manganites that bipolaron formation of (Mn<sup>3.5+</sup>)<sub>2</sub> units averages out the Mn–O bond lengths and leads to a narrower Mn–O bond length distribution than would be observed for a combination of Mn<sup>3+</sup> and Mn<sup>4+</sup>.<sup>11</sup> Based on the same principles, the (Mn<sup>3.33+</sup>)<sub>3</sub> trimers in TbBaMn<sub>2</sub>O<sub>5.75</sub> would be expected to have a fairly narrow Mn–O bond length distribution. This leaves only 25% of the Mn in the +3 oxidation state, which is low enough that most of these Mn could become 5 coordinate if the oxygen vacancies preferentially locate around them. This picture provides the first fully satisfactory explanation for why the superstructure of this compound differs so little from the ideal structure type despite its complexity.

It should also be noted that the tripolaron model is perfectly consistent with our SAED and HRTEM results<sup>23</sup>: the CO model consists of one Mn<sup>3+</sup> stripe alternating with three stripes of a (Mn<sup>3.33+</sup>)<sub>3</sub> trimer along the [101]<sub>p</sub> direction, giving a  $2\sqrt{2}a_p$  periodicity along this direction. This CO model was originally assigned as Mn<sup>4+</sup> and Mn<sup>3+</sup> respectively, based on an average Mn oxidation state of 3.25. To match the polaron model the oxidation states just need to be reassigned (Fig. S5). This implies that the oxygen vacancies could be expected to be associated with the narrower stripes, opposite of where they would be expected for the model with 3:1 charge ordering of Mn<sup>3+</sup> and Mn<sup>4+</sup> and exclusively located within the Tb layers as it was revealed by exit wave reconstruction of HRTEM images.

#### 4. Conclusions

Magnetic studies of TbBaMn<sub>2</sub>O<sub>5.75</sub> have revealed new aspects of the electronic structure of this compounds that were not apparent from crystallographic studies alone. A new pattern of polaron formation is suggested to occur in TbBaMn<sub>2</sub>O<sub>5.75</sub> which consists of S=11/2 (Mn<sup>3.33+</sup>)<sub>3</sub> trimers and isolated Mn<sup>3+</sup>. The charge ordering in this compound is unusual in that it displays both bond centered charge ordering within the tripolarons as well as site centered charge ordering on the Mn<sup>3+</sup>. This study also shows how small changes in oxygen content in layered RBaMn<sub>2</sub>O<sub>6-x</sub> compounds can fundamentally change their properties. Understanding the details of the charge ordering in compounds such as TbBaMn<sub>2</sub>O<sub>5.75</sub> is essential for understanding how to develop multiferroics with strong magnetoelectric coupling.

**Acknowledgements:** This work has benefited from the use of HIPD at the Lujan Center at Los Alamos Neutron Science Center, funded by DOE Office of Basic Energy Sciences. Los Alamos National Laboratory is operated by Los Alamos National Security LLC under DOE Contract DE-AC52-06NA25396. S.G.-M.thanks the Spanish MEC for funding Project MAT2010-19837-C06-03, MAT2013-46452-C4-4-R and the EC for SOPRANO. FP7-PEOPLE-2007-1-1-ITN. We thank Subakti for preparing the sample and Dr. Julio Romero for collecting the magnetic data.

Magnetic Phase	T range (K)	CW T fit range (K)	C (emuK/molOe)	$\mu_{\text{eff}}/\mu_{\text{B}}$	$\theta$ (K)
CM PM	457-699+	501-699	28.27(3)	15.04(2)	+196.4(8)
CO PM	203-457	224-299	42.74(8)	18.49(3)	-75.6(5)
Mn AFM / Tb PM	11-203	61-126	29.6(2)	15.4(1)	-11.4(5)
Mn + Tb AFM	Below 11				

Table 1. Magnetic data for the four phases of  $\text{TbBaMn}_2\text{O}_{5.75}$ . All moments are reported per a  $\text{Tb}_2\text{Ba}_2\text{Mn}_4\text{O}_{11.5}$  formula unit.

T (K)	$a$ (Å)	$c$ (Å)
300	3.9025(2)	7.5925(3)
240	3.9019(2)	7.5830(3)
200	3.9019(2)	7.5761(3)
175	3.9024(2)	7.5716(3)
150	3.9021(2)	7.5685(3)
125	3.9019(2)	7.5656(4)
100	3.9017(2)	7.5635(4)
70	3.9015(2)	7.5616(4)
52	3.9014(2)	7.5610(4)
40	3.9014(2)	7.5610(4)
30	3.9014(2)	7.5610(4)
20	3.9014(2)	7.5609(4)
15	3.9013(2)	7.5608(4)
10	3.9014(2)	7.5607(4)
4	3.9013(2)	7.5591(3)

Table 2. Evolution of the tetragonal subcell lattice parameters of  $\text{TbBaMn}_2\text{O}_{5.75}$  with temperature from fitting of the NPD patterns.

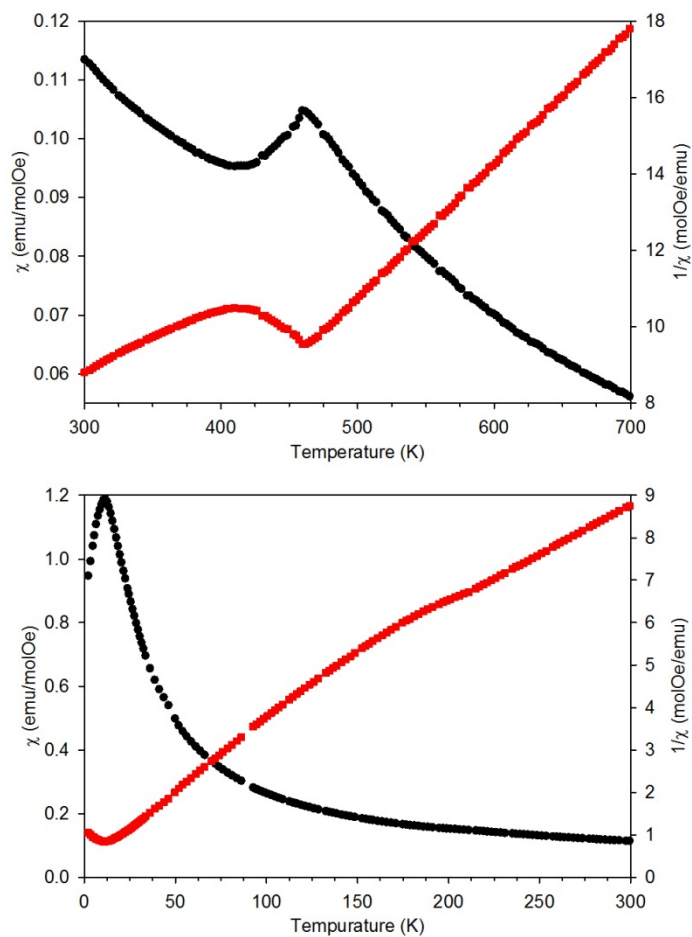


Figure 1. Magnetic susceptibility (black circles, left y-axis) and inverse magnetic susceptibility (red squares, right y-axis) vs. temperature plots for  $\text{TbBaMn}_2\text{O}_{5.75}$  over two temperature ranges.

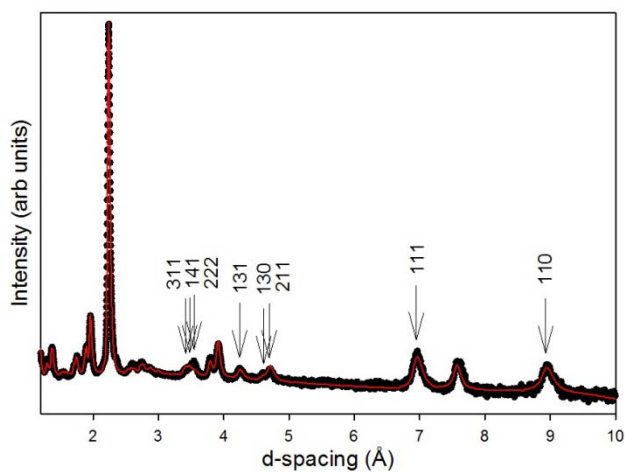


Figure 2. The NPD pattern (bank 5,  $40^\circ$ ) of  $\text{TbBaMn}_2\text{O}_{5.75}$  at 52 K (black circles) and the fit (red line). Arrows mark all magnetic peaks above  $3.2 \text{ \AA}$  with the  $hkl$  indices above them.

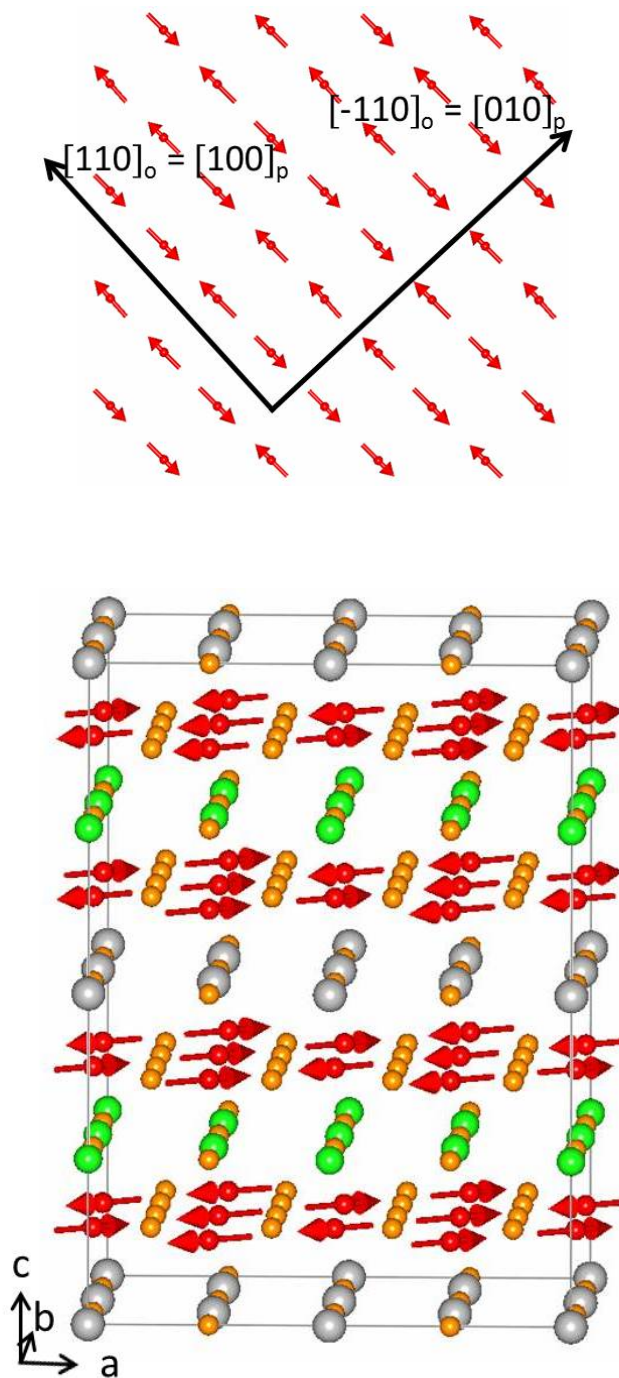


Figure 3. The top figure shows  $2 \times 2$  unit cells in the  $ab$ -plane, illustrating the  $\uparrow\uparrow\downarrow$  and  $\downarrow\downarrow\uparrow$  pattern of spins along the  $[110]$  and  $[-110]$  directions. Only the Mn atoms and their moments are shown. The bottom figure shows the crystal and magnetic structure of  $\text{TbBaMn}_2\text{O}_{5.75}$  at 52 K. Large green atoms are Tb, large gray atoms are Ba, small orange atoms are oxygen, and small red atoms are Mn. The red arrows represent the ordered magnetic moments on the Mn.

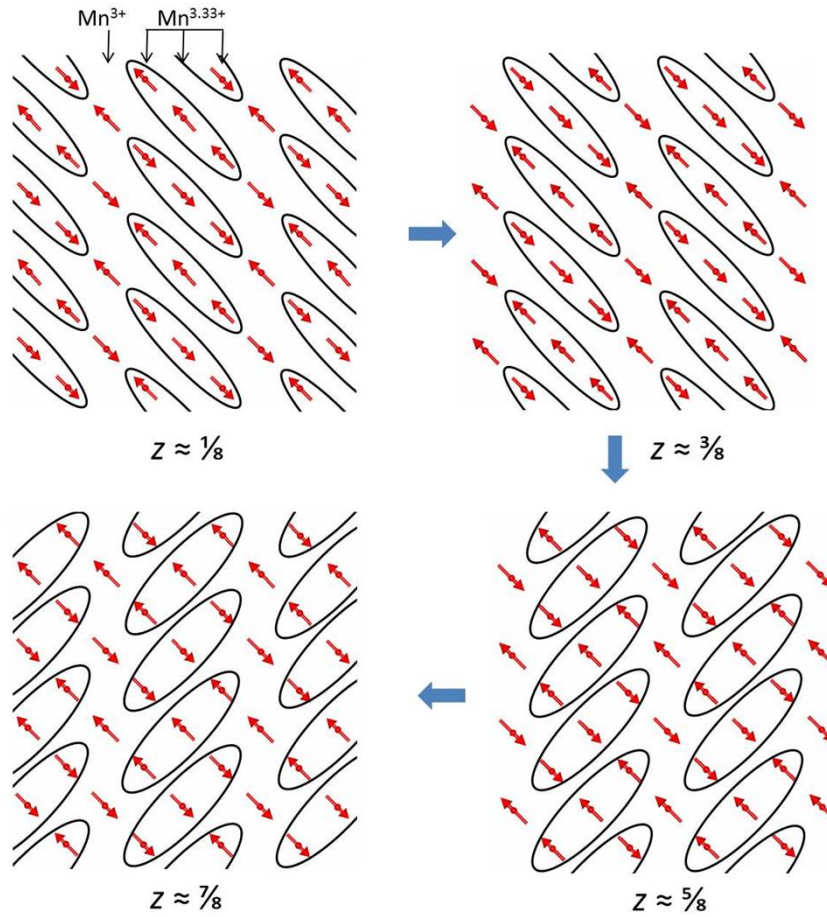


Figure 4. Tripolaron formation in  $\text{TbBaMn}_2\text{O}_{5.75}$ . Each picture shows  $2 \times 2$  unit cells in the  $ab$ -plane for different Mn layers along the  $z$ -axis. Only Mn atoms and their moments are shown. The atoms enclosed within ovals are FM coupled trimers while atoms not in ovals are  $\text{Mn}^{3+}$ .

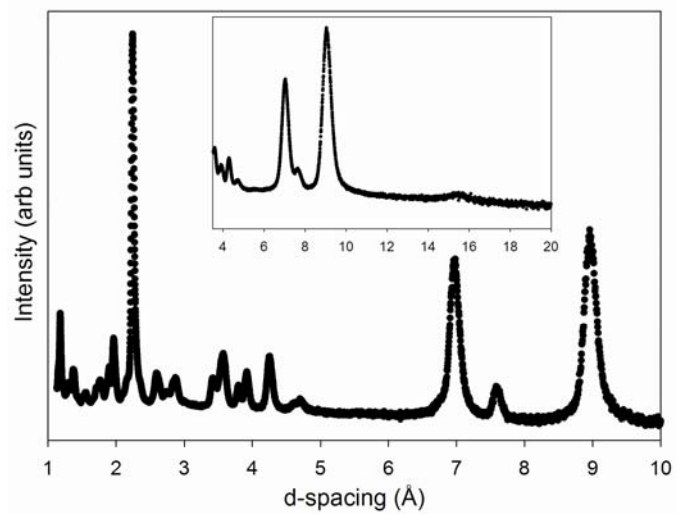


Figure 5. The NPD pattern of TbBaMn<sub>2</sub>O<sub>5.75</sub> at 4 K. The main figure shows the data from bank 5 (40°) and the bank 7 (14°) data is shown in the insert.

## References:

- 1) S. Dong and J.-M. Liu, *Mod. Phys. Lett. B* **26**, 1230004 (2012).
- 2) K. F. Wang, J.-M. Liu, and Z. F. Ren, *Advances in Physics* **58**, 321 (2009).
- 3) D. I. Khomskii, *J. Mag. Mag. Mater.* **306**, 1 (2006).
- 4) W. Eerenstein, N. D. Mathur, and J. F. Scott, *Nature* **442**, 759 (2006).
- 5) N. A. Hill, *J. Phys. Chem. B* **104**, 6694 (2000).
- 6) C. N. R. Rao, and C. R. Serrao, *J. Mater. Chem.* **17**, 4931 (2007).
- 7) S.-W. Cheong, and M. Mostovoy, *Nature Materials* **6**, 13 (2007).
- 8) M. Mostovoy, *Phys. Rev. Lett.* **96**, 067601 (2006).
- 9) T. Kimura, *Annu. Rev. Mater. Res.* **37**, 387 (2007).
- 10) D. V. Efremov, J. van den Brink and D. I. Khomskii, *Nat. Mater.* **3**, 853, 2004.
- 11) A. Daoud-Aladine, J. Rodriguez-Carvajal, L. Pinsard-Gaudart, M. T. Fernandez-Diaz, A. Revcolevschi, *Phys. Rev. Lett.*, **89**, 097205 (2002).
- 12) C. R. Serrao, A. Sundaresan and C. N. R. Rao, *J. Phys.: Condens. Matter* **19** (2007) 496217.
- 13) S. Sagar, P. A. Joy and M. R. Anantharaman, *Ferroelectrics*, 392, 13, 2009.
- 14) T. Nakajima, H. Kageyama, H. Yoshizawa, Y. Ueda, *J. Phys. Soc. Japan* **2002**, *71*, 2843.
- 15) T. Nakajima, H. Kageyama, H. Yoshizawa, K. Ohoyama, *J. Phys. Soc. Japan* **2003**, *72*, 3237.
- 16) Y. Ueda, T. Nakajima, *J. Phys. Condens. Matter* **2004**, *1*, S573.
- 17) M. Uchida, D. Akahoshi, R. Kumai, Y. Tomioka, T. Arima, T. Tokura, Y. Matsui, *J. Phys. Soc. Japan* **2002**, *71*, 2605.
- 18) T. Arima, D. Akahoshi, K. Oikawa, T. Kamirama, M. Uchida, Y. Matsui, T. Tokura, *Phys. Rev. B.* **2002**, *66*, 140408.
- 19) A. J. Williams, J. P. Attfield, *Phys. Rev. B.* **2002**, *66*, 220405(R).
- 20) H. Kageyama, T. Nakajima, M. Ichihara, Y. Ueda, H. Yoshizawa, K. Ohoyama, *J. Phys. Soc. Japan* **2003**, *72*, 241.
- 21) A. J. Williams, J. P. Attfield, *Phys. Rev. B.* **2005**, *72*, 024436.

- 22) D. Akahoshi, Y. Okimoto, M. Kubota, R. Kumai, T. Arima, Y. Tomioka, Y. Tokura, *Phys. Rev. B.* **2004**, *70*, 064418.
- 23) D. Avila-Brandé, G. King, E. Urones-Garrote, Subakti, A. Llobet, and S. Garcia-Martin, *Adv. Funct. Mater.*, **24**, 2510-2517 (2014).
- 24) A. C. Larson and R. B. Von Dreele, Los Alamos National Laboratory Report No. LAUR 86-748, 2004.
- 25) B. H. Toby, *J. Appl. Crystallogr.* **34**, 210 (2001).
- 26) A. S. Wills, *Physica B* 276–278, **680**, 2000; program available at [www.ccp14.ac.uk](http://www.ccp14.ac.uk)
- 27) See Supplemental Material at [URL will be inserted by publisher] for additional figures.
- 28) E. L. Winkler, M. Tovar, M. T. Causa, *J. Phys.: Condens. Matter*, **25**, 296003 (2013).
- 29) G. King, S. Thimmaiah, A. Dwivedi, P. M. Woodward, *Chem. Mater.*, **19**, 6451 (2007).
- 30) G. King, L. M. Wayman, P. M. Woodward, *J. Solid State Chem.*, **182**, 1319 (2009).
- 31) G. King, A. S. Wills, P. M. Woodward, *Phys. Rev. B*, **79**, 224428 (2009).
- 32) G. Zheng, C. H. Patterson, *Phys. Rev. B*, **67**, 220404 (2003).
- 33) A. Daoud-Aladine, C. Perca, L. Pinsard-Gaudart, J. Rodriguez-Carvajal, *Phys. Rev. Lett.*, **101**, 166404 (2008).
- 34) M. Garcia-Fernandez, U. Staub, Y. Bodenthin, S. M. Lawrence, A. M. Mulders, C. E. Buckley, S. Weyeneth, E. Pomjakushina, K. Conder, *Phys. Rev. B*, **77**, 060402 (2008).
- 35) M. Garcia-Fernandez, U. Staub, Y. Bodenthin, V. Scagnoli, V. Pomjakushin, S. W. Lovesey, A. Mirone, J. Herrero-Martin, C. Piamonteze, E. Pomjakushina, *Phys. Rev. Lett.*, **103**, 097205 (2009).
- 36) P. Schiffer, A. P. Ramirez, W. Bao, S. W. Cheong, *Phys. Rev. Lett.*, **18**, 3336 (1995).
- 37) J. L. Garcia-Munoz, C. Frontera, A. Llobet, A. E. Carrillo, A. Caneiro, M. A. G. Aranda, C. Ritter, E. Dooryee, *Physica B*, **350**, e277-e279 (2004).

TOC Graphic:

